

First-Principles Study of Mg-Induced Phase Stabilization in Ga_2O_3 polymorphs

Viswesh Prakash, Jingyu Tang, Lisa M. Porter, and Rachel C. Kurchin*

Department of Materials Science and Engineering, Carnegie Mellon University, Pittsburgh, Pennsylvania 15213, USA

E-mail: rkurchin@cmu.edu

Abstract

In this study, we investigate the effect of Mg incorporation on the relative phase stability of the four primary Ga_2O_3 polymorphs using density functional theory (DFT) calculations, with the goal of rationalizing experimental observations suggesting that diffusion from MgAl_2O_4 substrates contributes to relative stabilization of the γ phase. Mg incorporation is modeled up to 25% of Ga sites within supercells derived from fully relaxed unit cells of each polymorph. Our results show that while β - Ga_2O_3 remains the thermodynamically most stable phase, the enthalpic differences between polymorphs decrease with increasing Mg content. The inherently disordered γ phase, with its high configurational entropy, becomes less energetically unfavorable under Mg substitution, suggesting that entropy-driven stabilization may facilitate its formation under high-temperature and/or nonequilibrium growth conditions such as those previously reported. These findings provide a thermodynamic rationale for the experimental observation of the γ phase during epitaxial growth on MgAl_2O_4 spinel substrates.

Introduction

Gallium oxide (Ga_2O_3) has emerged as a material of considerable interest for high-power electronic applications, owing to its ultra-wide bandgap, high breakdown field, and potential for efficient power device performance.^{1–4} Ga_2O_3 has four widely accepted polymorphs showing the following symmetries: α (trigonal), β (monoclinic), γ (cubic), and κ (also referred to as ϵ , orthorhombic). Among these, $\beta\text{-}\text{Ga}_2\text{O}_3$ is the thermodynamically stable phase,⁵ while $\gamma\text{-}\text{Ga}_2\text{O}_3$ is consistently identified as the least stable based on density functional theory (DFT) calculations.^{6,7}

Despite its theoretical instability, the γ phase is frequently observed in experimental studies. Notably, the $\gamma\text{-}\text{Ga}_2\text{O}_3$ phase has been reported to form as inclusions during the epitaxial growth of $\beta\text{-}\text{Ga}_2\text{O}_3$ films on $\beta\text{-}\text{Ga}_2\text{O}_3$ substrates, particularly when alloyed with Al_2O_3 or following ion implantation.^{8,9} Additionally, thin $\gamma\text{-}\text{Ga}_2\text{O}_3$ layers—typically on the order of a few tens of nanometers—have been detected at the interfaces of $\beta\text{-}\text{Ga}_2\text{O}_3$ films grown on MgO substrates with various crystallographic orientations, including (001), (011), and (111).^{10,11} These observations suggest that specific growth conditions and substrate interactions can kinetically favor the formation of the metastable γ phase.

Experimental evidence also indicates that the incorporation of certain elements during film growth can contribute to the stabilization of the γ phase. In particular, the addition of Mg ,^{12–14} Al ,¹⁵ Mn ,^{16–18} Fe ,¹⁹ or Cu ²⁰ has been found to promote the formation or retention of the γ phase. Our previous studies revealed the sequence of $\gamma\text{-}\text{Ga}_2\text{O}_3 \rightarrow \beta\text{-}\text{Ga}_2\text{O}_3 \rightarrow \gamma\text{-}\text{Ga}_2\text{O}_3$ solid solution on (100)-oriented MgAl_2O_4 substrates grown by metal-organic chemical vapor deposition (MOCVD) as growth temperature is increased. Specifically, $\gamma\text{-}\text{Ga}_2\text{O}_3$ formed at 470 °C, followed by the emergence of $\beta\text{-}\text{Ga}_2\text{O}_3$ in the temperature range of 530–650 °C. At higher growth or annealing temperatures (>750 °C), substantial Mg and Al diffusion occurred, leading to the formation of a $\gamma\text{-}\text{Ga}_2\text{O}_3$ solid-solution.^{14,21,22} Scanning transmission electron microscopy (STEM) analyses conducted across the substrate/thin-film interfaces of these films are shown in Figure 1. In this figure, it can be observed that at the intermediate

growth temperature ($750\text{ }^{\circ}\text{C}$), $\beta\text{-Ga}_2\text{O}_3$ becomes the preferred phase in the upper portion of the film where Mg and Al incorporation is negligible, while a transition layer below with substantial Mg and Al incorporation exhibits the γ structure. However, by $850\text{ }^{\circ}\text{C}$, diffusion is fast enough that this β layer is no longer present, and γ phase solid solution is stabilized throughout the film. More detailed growth conditions and structural characterizations of these films can be found in our previous publications.^{14,21,22}

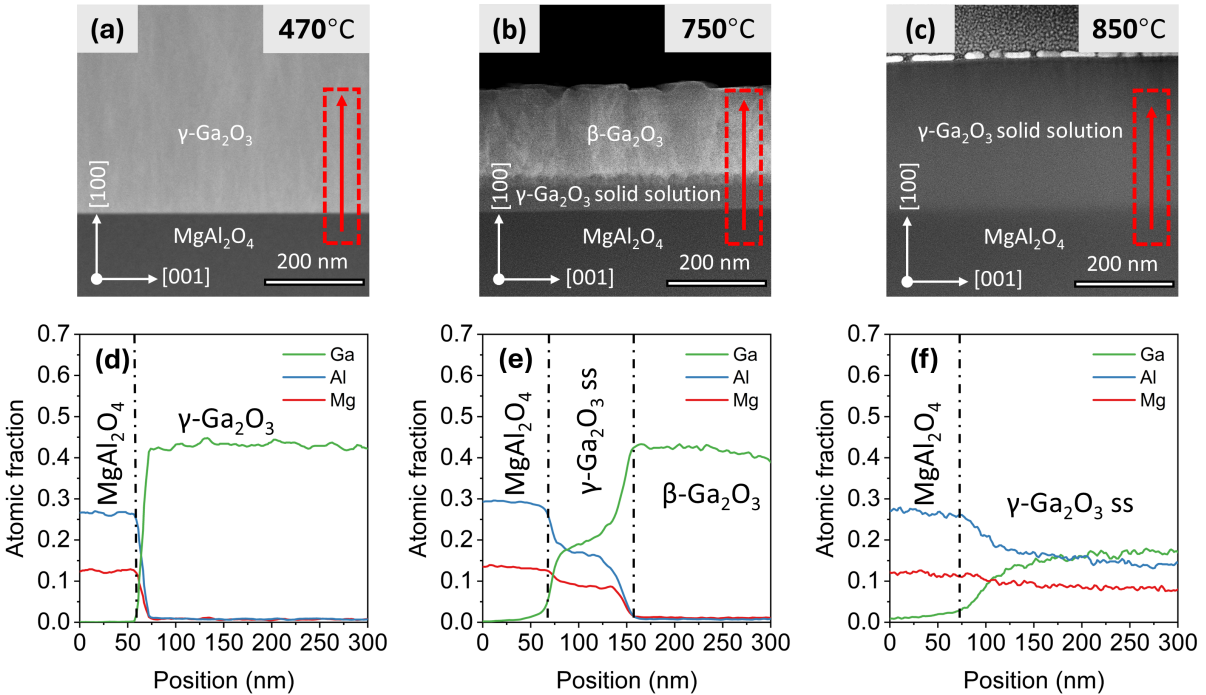


Figure 1: Cross-sectional high-angle annular dark-field scanning transmission electron microscopy (HAADF-STEM) images of films grown at (a) $470\text{ }^{\circ}\text{C}$, (b) $750\text{ }^{\circ}\text{C}$, and (c) $850\text{ }^{\circ}\text{C}$, respectively and their corresponding integrated EDX composition profiles shown in (d-f). The red dashed rectangles with arrows indicate the regions and directions along which the EDX profiles were acquired.

Further evidence for the role of MgAl₂O₄ substrates in stabilizing the γ phase has been provided by Oshima et al.²³ That study reports X-ray diffraction peak shifts indicative of diffusion-stabilized $\gamma\text{-Ga}_2\text{O}_3$ formation in films grown via mist chemical vapor deposition (mist-CVD) on (100)-oriented MgAl₂O₄. Hou et al.^{12,13} also reported the successful growth of (111)-oriented, phase-pure Mg_xGa₂O₄ inverse spinel films on (0001) sapphire substrates, without the formation of the β phase. Furthermore, they observed that post-growth anneal-

ing at 900 °C led to improved structural ordering without inducing a phase transformation to the β structure.

In addition to experimental demonstrations,^{15,24} theoretical analyses indicate that the γ phase can become the dominant structural form in $(\text{Al}_x\text{Ga}_{1-x})_2\text{O}_3$ films depending on the Al concentration and specific growth technique employed. Several computational studies have sought to elucidate the effects of alloying on the phase stability of Ga_2O_3 polymorphs. Peelaers et al.²⁵ investigated the relative stability of monoclinic (β) and corundum (α) $(\text{Al}_x\text{Ga}_{1-x})_2\text{O}_3$ alloys at zero temperature, while Seacat et al.²⁶ extended this analysis to the orthorhombic (κ) phase. Mu and Van de Walle²⁷ conducted a comprehensive analysis of Al incorporation into all known Ga_2O_3 polymorphs, demonstrating that alloying with Al significantly reduces the energy difference between the γ - and β phases, thereby enhancing the metastability of $\gamma\text{-Ga}_2\text{O}_3$.

While the stabilizing effect of Al alloying on the γ phase has been explored in detail, experimental observations suggest that both Al and Mg play critical roles in stabilizing the γ phase under specific growth conditions. However, the independent influence of Mg incorporation on the phase stability of Ga_2O_3 polymorphs remains an open question and is largely unaddressed in the existing literature.

The present study seeks to address this gap by employing a first-principles computational approach based on density functional theory. We investigate the relative phase stability of all four Ga_2O_3 polymorphs— α , β , γ , and κ —in $(\text{Mg}_x\text{Ga}_{1-x})_2\text{O}_{3-x}$ alloys at zero temperature. Through this work, we aim to clarify the thermodynamic role of Mg incorporation in stabilizing the metastable γ phase and to contribute a more complete understanding of the compositional factors that govern polymorph formation in Ga_2O_3 -based materials.

Methodology

Structures of Polymorphs

In this study, we focus on the four commonly accepted polymorphs of Ga_2O_3 — β (monoclinic), κ (orthorhombic), α (trigonal), and γ (cubic)—as well as the MgO structure, which adopts a cubic rock-salt configuration. Among these Ga_2O_3 polymorphs, the γ phase is characterized by a disordered structure,^{7,28} where cation vacancies can occupy both tetrahedral and octahedral sites in the defective spinel structure. Hence the unit cell of $\gamma\text{-Ga}_2\text{O}_3$ was constructed following the two-step process outlined in the literature.^{6,27,29} First, a triclinic supercell was derived from the conventional cubic spinel cell corresponding to the stoichiometry Ga_3O_4 by applying a lattice transformation to the lattice vectors $(\vec{a}_0, \vec{b}_0, \vec{c}_0)$ as follows:

$$\begin{pmatrix} \vec{a}' \\ \vec{b}' \\ \vec{c}' \end{pmatrix} = \begin{pmatrix} 0.5 & 0.5 & 0 \\ 0 & 0.5 & 0.5 \\ 1.5 & 0 & 1.5 \end{pmatrix} \begin{pmatrix} \vec{a}_0 \\ \vec{b}_0 \\ \vec{c}_0 \end{pmatrix} \quad (1)$$

Subsequently, two Ga atoms were selectively removed from octahedral sites in the transformed triclinic cell, thereby yielding the desired stoichiometry of Ga_2O_3 . These Ga atoms were chosen such that they are separated by a distance of approximately 7.9 Å. The unit cells for all the Ga_2O_3 polymorphs are illustrated in Figure 2. The types of cation and anion sites characteristic of each polymorph are summarized in Table 1.

To examine the effects of Mg incorporation, we construct alloyed structures by substituting Ga atoms with Mg within supercells derived from the respective unit cells shown in Figure 2. At each specified Mg concentration, various configurations can be generated by selectively replacing Ga atoms occupying distinct cation sites. To preserve charge balance, oxygen vacancies are introduced alongside Mg substitution (see Computational Details for more information). In this study, we restrict the extent of Mg substitution to a maximum of 25% of the available Ga sites.

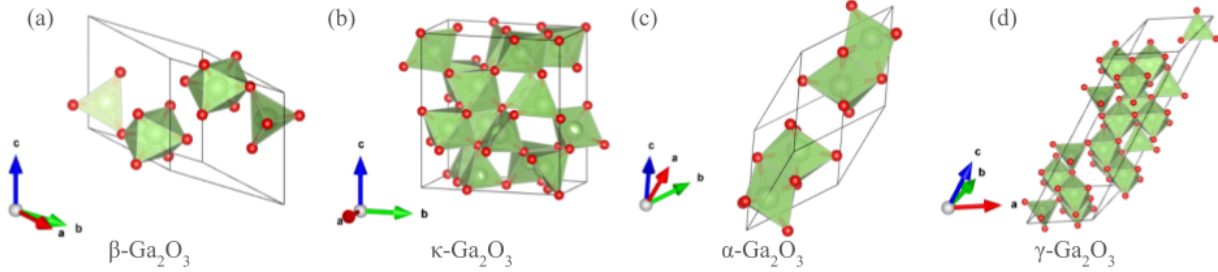


Figure 2: Illustration of structures for Ga_2O_3 polymorphs in decreasing order of stability as determined by DFT – (a) $\beta\text{-}\text{Ga}_2\text{O}_3$; (b) $\kappa\text{-}\text{Ga}_2\text{O}_3$; (c) $\alpha\text{-}\text{Ga}_2\text{O}_3$; (d) $\gamma\text{-}\text{Ga}_2\text{O}_3$. Red spheres denote O atoms and green spheres and polyhedra denote Ga atoms and their coordination. Cells (a) and (c) are primitive unit cells of the respective structures. Structural visualization was performed using VESTA.³⁰

Table 1: Summary of Ga coordination and O site connectivity for structures of all Ga_2O_3 polymorphs.

Structure	Ga site ratio (octahedral:tetrahedral)	Types of O sites [O at corners of polyhedra]
β	1:1	Edge sharing between octahedra Corner sharing between tetrahedra Corner sharing between octahedra and tetrahedra
κ	3:1	Edge sharing between octahedra Corner sharing between tetrahedra Corner sharing between octahedra and tetrahedra
α	All octahedral	Edge sharing between octahedra
γ	5:3	Edge sharing between octahedra Corner sharing between tetrahedra Corner sharing between octahedra and tetrahedra

Computational Details

All first-principles calculations were performed using DFT within the projector augmented-wave³¹ (PAW) formalism as implemented in the Quantum ESPRESSO package. The exchange-correlation interactions were described using the generalized gradient approximation (GGA) as formulated by Perdew, Burke, and Ernzerhof (PBE).³² Prior to structural relaxations, convergence tests were carried out to determine appropriate values for the plane-wave kinetic energy cutoff, the charge density kinetic energy cutoff, and the Brillouin-zone sampling mesh. Based on these tests, the plane-wave energy cutoff was fixed at 140 Ry, and the charge density cutoff was set to 560 Ry. Brillouin-zone integrations were performed using a Γ -centered Monkhorst–Pack $6\times 6\times 6$ k-point mesh for the primitive cells of the monoclinic β and trigonal α phases, a $6\times 4\times 4$ mesh for the orthorhombic κ phase, and a $6\times 6\times 2$ mesh for the triclinic cell of the defective spinel γ phase. All polymorphs were fully relaxed with respect to both atomic positions and lattice parameters. The resulting optimized structural parameters are summarized in Table 2 and are in good agreement with experimentally reported values.

To minimize the effects of short-range ordering induced by periodic boundary conditions in DFT calculations of substitutional alloys, supercells were constructed for all polymorphs based on the respective unit cells shown in Figure 2. Furthermore, to avoid ordering along specific lattice directions, supercells were constructed using lattice transformation matrices that yield approximately cubic supercells with a comparable distribution of Ga sites along each axis of the supercell. These lattice transformations are carried out as follows:

$$\begin{pmatrix} \vec{a}' \\ \vec{b}' \\ \vec{c}' \end{pmatrix} = A_{sc} \begin{pmatrix} \vec{a} \\ \vec{b} \\ \vec{c} \end{pmatrix} \quad (2)$$

Where \vec{a} , \vec{b} , and \vec{c} are the lattice vectors of the primitive cell, A_{sc} is the integer lattice transformation matrix, and \vec{a}' , \vec{b}' , and \vec{c}' are the resulting lattice vectors of the generated

Table 2: DFT-relaxed structural parameters for all polymorphs of Ga_2O_3 in comparison to experimentally determined lattice parameters. Lattice parameters in Å and angles in degrees.

	Experimental	Calculated
Mononclinic (β) ³³		
a	12.2	12.4565
b	3.0	3.085
c	5.8	5.879
beta	104	103.688
Trigonal (α) ³⁴		
a	4.98	5.0597
c	13.43	13.6283
Orthorhombic (κ) ³⁵		
a	5.0	5.1243
b	8.68	8.8023
c	9.23	9.4124
Defective spinel (γ) ²⁸		
a	8.24	8.325

supercell, expressed as linear combinations of the original lattice vectors.

The lattice transformation matrices used for the β , α , and κ phases are as follows:

$$A_\beta = \begin{pmatrix} 2 & 0 & 0 \\ -4 & 4 & 0 \\ 0 & 0 & 2 \end{pmatrix}$$

$$A_\alpha = \begin{pmatrix} 2 & 0 & 0 \\ -1 & 3 & -1 \\ -1 & -1 & 3 \end{pmatrix}$$

$$A_\kappa = \begin{pmatrix} 2 & 0 & 0 \\ 0 & 1 & 0 \\ 0 & 0 & 1 \end{pmatrix}$$

For the defective spinel γ -Ga₂O₃ having a primitive cell showing triclinic symmetry, we adopt the method of constructing an oriented bulk structure as described by Sun and Ceder,³⁶ to ensure that the out-of-plane lattice vector aligns with experimentally observed orientations. The resulting transformation matrix from this approach is:

$$A_\gamma = \begin{pmatrix} 0 & 2 & 0 \\ -3 & 0 & 1 \\ 2 & -1 & 0 \end{pmatrix}$$

Applying the aforementioned lattice transformations to the unit cells results in supercells containing 160 atoms for the β , α , and γ polymorphs, and 80 atoms for the κ polymorph. These supercells serve as the basis for modeling Mg incorporation into the Ga₂O₃ lattice by substituting Ga atoms with Mg. Since Mg²⁺ has a lower valence state than Ga³⁺, charge compensation is required to maintain overall neutrality. This is achieved by introducing one oxygen vacancy for every two Ga sites substituted with Mg. Thus, the alloyed compositions studied in this work follow the general formula (Mg_xGa_{1-x})₂O_{3-x}.

Mg substitution was explored both with and without cation site preference, i.e. Mg atoms are substituted at Ga sites both at random and by restricting to Ga atoms occupying a specific cation site (octahedral or tetrahedral). However, given the combinatorially large number of possible configurations—for instance, at 25% of Ga site having Mg substitution, there are over 10¹⁴ possible configurations when symmetry equivalence between arrangements is not considered—an exhaustive computational study of all configurations is

impractical. To address this, we define structural equivalence using a geometric criterion: two configurations are considered symmetrically equivalent if the set of all pairwise distances among Mg atoms, among oxygen vacancies, and between Mg and vacancy sites are identical. After this symmetry-based filtering is applied, the number of inequivalent configurations is reduced at lower concentration of Mg substitution. Nevertheless, for the range of concentrations (6.25% to 25%) considered in this study, the number of inequivalent configurations remains substantial. Due to the computational cost associated with performing full DFT relaxations for all inequivalent structures, it is necessary to select a representative subset of configurations at each concentration for further investigation.

To select a representative subset of configurations for a given polymorph and Mg concentration, we adopt a statistical approach based on radial distribution functions (RDFs). Initially, a large number of symmetrically inequivalent structures are generated. By computing all partial RDF's between species within the structure and comparing results from subsets to averages over the full ensemble, we can select a subset that retains acceptable representation of the full range of environments. For more details, see the Supporting Information.

The thermodynamic stability of the Mg-incorporated structures at zero temperature is evaluated through the calculation of their enthalpies of formation (ΔH). This is done by referencing the total energies of the substituted structures to the most stable phases of the constituent binary oxides—namely, β -Ga₂O₃ and MgO. The formation enthalpy for a given composition of the alloyed system $(\text{Mg}_x\text{Ga}_{1-x})_2\text{O}_{3-x}$ is computed according to the following expression (where $E[\dots]$ refers to DFT total energy):

$$\Delta H[(\text{Mg}_x\text{Ga}_{1-x})_2\text{O}_{3-x}] = E[(\text{Mg}_x\text{Ga}_{1-x})_2\text{O}_{3-x}] - (1-x)E[\text{Ga}_2\text{O}_3] - 2xE[\text{MgO}] \quad (3)$$

Results and Discussion

The phase stability of the different Ga_2O_3 polymorphs was assessed by comparing their enthalpies of formation (ΔH). Our results for the unsubstituted Ga_2O_3 structures agree with previous calculations⁶ and the relative phase stability follows the expected trend, in order of increasing ΔH : $\beta < \kappa < \alpha < \gamma$. The γ phase, as anticipated, is the least stable, with a ΔH of 0.222 eV/f.u.—significantly higher than those of the α phase ($\Delta H = 0.153$ eV/f.u.) and κ phase ($\Delta H = 0.106$ eV/f.u.), all referenced to the β phase. Our calculated ΔH values are consistent with prior literature,^{25–27} deviating by ~ 0.01 eV/f.u. Figure 3 presents the minimum ΔH values for the β , κ , and α polymorphs as a function of Mg substitution on Ga sites, without cell shape relaxation. From Figure 3, we note that as the Mg concentration increases, the differences in enthalpy of formation across the polymorphs decrease with increasing concentration of Mg. This suggests that Mg incorporation reduces the energetic penalty for forming the metastable polymorphs, rendering them more competitive in energy with the thermodynamically stable β phase. Consequently, the addition of Mg may make the metastable polymorphs energetically accessible structures that can be grown by tuning the growth conditions, where the influence of kinetics, strain or co-doping effects of other atoms could further stabilize the different polymorphs.

Given that both the γ - and β phases have been experimentally observed to grow on Mg-containing substrates such as MgO and MgAl_2O_4 , we examine the effect of Mg substitution in these two polymorphs in greater detail. Specifically, we analyze the site preference and energetic impact of Mg incorporation across different substitution scenarios. To ensure relevance to experimentally observed growth conditions, these calculations are performed using epitaxially constrained structures, where the out-of-plane lattice vector that was allowed to relax is consistent with the experimentally reported out-of-plane normal for epitaxial growth (and the other two lattice vectors were fixed according to the epitaxial matching constraint). Our results indicate that in $\beta\text{-Ga}_2\text{O}_3$, Mg atoms show a clear preference to occupy octahedral Ga sites. Figure 4a shows the average and range of the enthalpy of formation for substituted

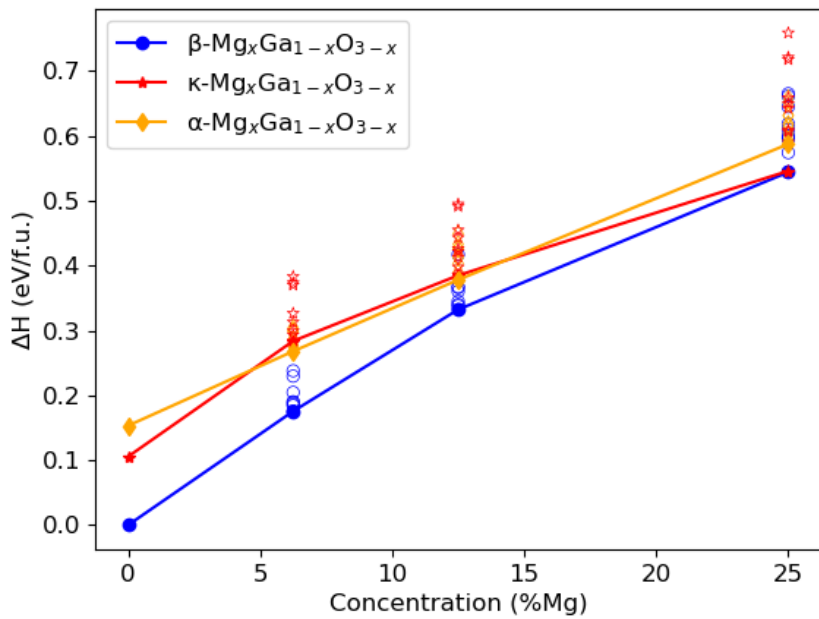


Figure 3: Bulk enthalpy of formation (ΔH) for $(\text{Mg}_x\text{Ga}_{1-x})_2\text{O}_{3-x}$ alloys as a function of Mg concentration (% of Ga sites substituted) for the α -, β -, and κ -polymorphs of Ga_2O_3 . Filled symbols represent minimum values, while open symbols represent the values for enthalpy of formation of other structures in the selected sample of structures for each polymorph at a given concentration.

β -Ga₂O₃ as a function of the Mg concentration, we see that the octahedral substitution of Mg significantly reduces the enthalpy of formation for the substituted structure at higher concentrations when compared to tetrahedral substitution or random substitution. In contrast, γ -Ga₂O₃ does not exhibit a strong site preference for Mg; the enthalpy of formation remains relatively insensitive to the specific site occupancy across the full range of Mg concentrations considered. This can be seen in Figure 4b, exhibiting no noticeable reduction in the enthalpy of formation for any given site occupancy of Mg in the γ structure.

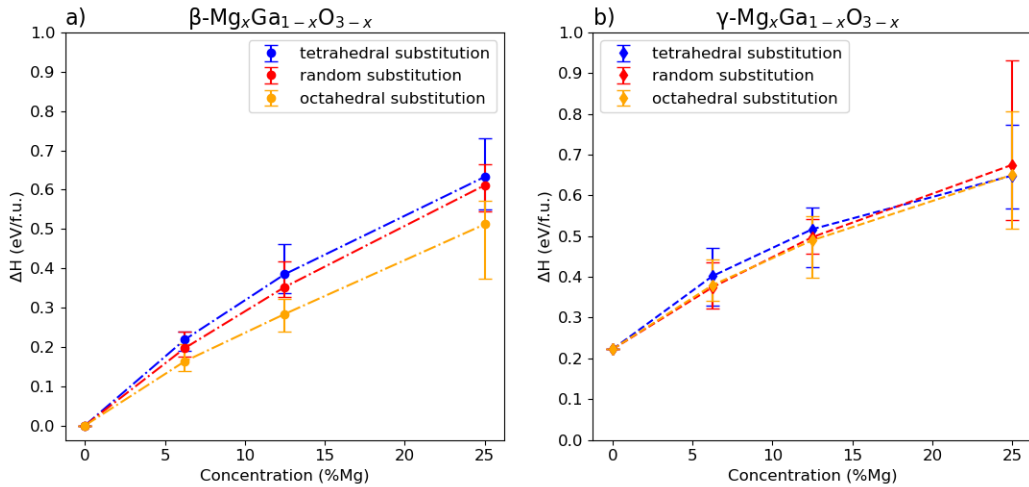


Figure 4: Average and range of enthalpy of formation (ΔH) for epitaxially strained Mg-substituted (a) β -Ga₂O₃ and (b) γ -Ga₂O₃ as a function of % Ga sites substituted, shown for three site occupancy configurations: octahedral-only (yellow), tetrahedral-only (blue), and random distribution (red).

To further understand the energetic relationship between the γ - and β -polymorphs during Mg substitution, we directly compare the enthalpy of formation for both polymorphs as a function of Mg concentration for the same three substitution configurations: octahedral-only, tetrahedral-only, and random occupancy (Figure S20). The key takeaway from this comparison is that, like in the relaxed bulk results shown in Figure 3, Mg incorporation also reduces the energy difference between the β and γ phases in these strained simulations.

Figures 5a-c show atomic-scale HAADF-STEM images of representative regions from the

same three films shown in Figure 1, all exhibiting structural features consistent with the spinel structure shown in Figure 5d. Three line profiles highlighted in orange, red and blue, each starting and ending at atoms on octahedral sites, were extracted from the images to evaluate the cation site preference based on the contrast difference between tetrahedral and octahedral sites, where the HAADF contrast is roughly $Z^{1.6}$ (where Z is the atomic number). The lighter Al and Mg atoms preferentially occupy octahedral Ga sites and the heavier Ga atoms prefer to be on tetrahedral sites, as observed by the inversion of the image intensity profiles (Figure 5e) for pure γ -Ga₂O₃ (Figure 5a, orange line in e) and γ -Ga₂O₃ solid solutions (Figure 5b-c, red/blue lines in e).

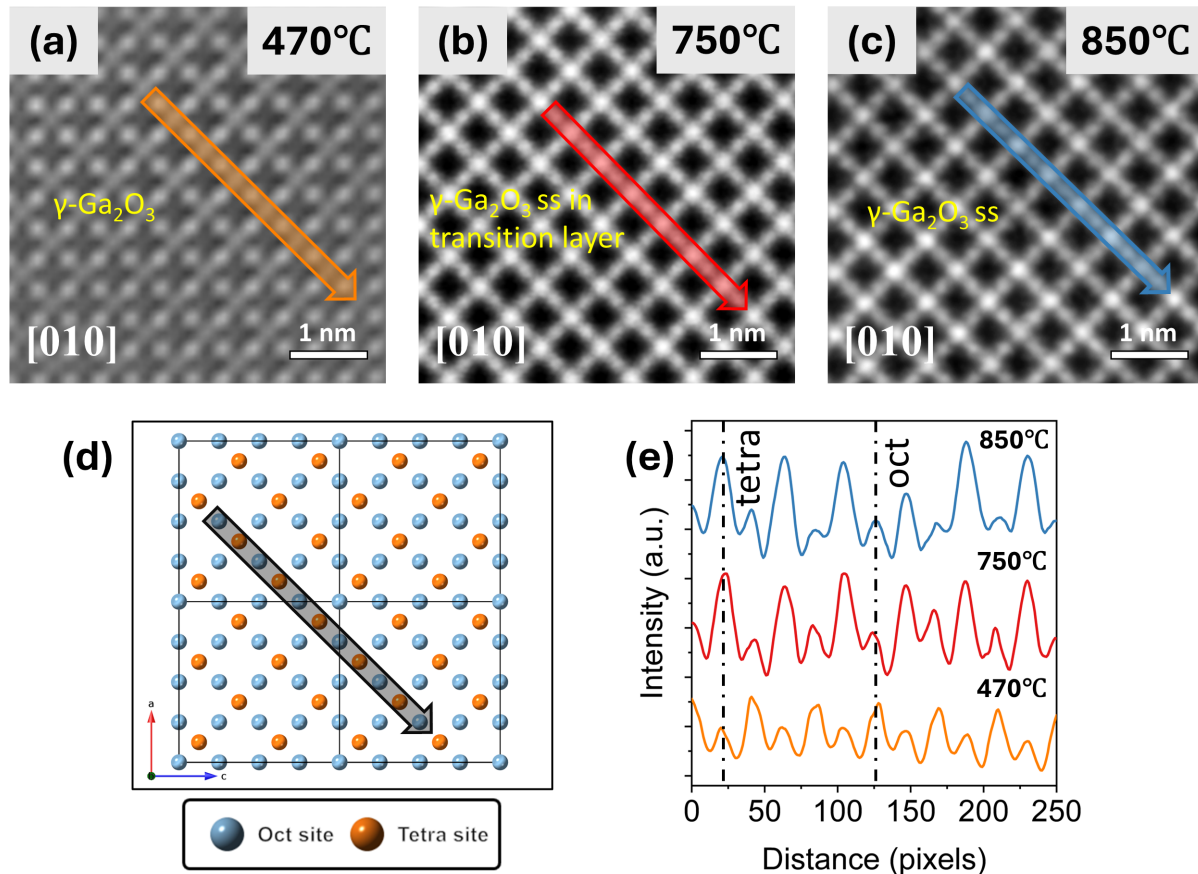


Figure 5: Atomic-scale HAADF-STEM images for the film grown at (a) 470 °C, (b) 750 °C and (c) 850 °C, respectively. (d) shows the atomic structure of cubic spinel structure along [010] zone. (e) shows the combined line profiles of the image intensity across three atomic rows from (a) to (c), showing the inversion in relative contrast between tetrahedral and octahedral sites.

In a study similar to the present work, Mu et al.²⁷ report that Al strongly prefers to occupy octahedral Ga sites in both β - and γ -Ga₂O₃, unlike the results reported here for Mg, where this preference is only present in the β phase. While Mg shows no strong site preference in γ -Ga₂O₃, its incorporation does reduce the enthalpy difference between the β and γ phases, and the diffusion of Al and Mg during growth collectively make the γ phase more energetically accessible. This is consistent with experimental observations that show Al preferentially occupies octahedral sites while Ga tends to occupy tetrahedral sites. Given that the γ phase contains a higher proportion of octahedral to tetrahedral sites (5:3), and Mg does not show a site preference, it is more likely to occupy an octahedral site while stabilizing the γ phase.

While the enthalpies of formation are discussed in this work, it is important to consider that free energy, rather than enthalpy alone, governs phase stability under real synthesis conditions. In particular, configurational entropy, which arises from the number of ways atoms can be arranged in a structure can play a significant role in stabilizing disordered or metastable phases at finite temperatures. The γ -Ga₂O₃ phase is inherently structurally disordered, characterized by a defective spinel lattice with partial occupancy of both tetrahedral and octahedral cation sites. When Mg is introduced into this already disordered framework, the number of possible configurations increases dramatically due to the variability in choosing Ga sites for substitution, resulting in a high configurational entropy. This entropy contribution ($S = k_B \ln(\Omega)$; where Ω is the number of distinct configurations) lowers the free energy of the γ phase relative to the other more ordered phases. This implies that high-temperature growth conditions or post-growth annealing treatments could thermodynamically favor the formation or persistence of the Mg-doped γ phase.

We note also that in this work, we have assumed that the γ phase remains “Ga₂O₃-like” – namely, that the cation:oxygen ratio remains approximately 2:3, with all deviations arising due to the additional vacancies introduced to preserve charge balance under Mg incorporation. In reality, experimental characterization suggests that at higher Mg and

Al incorporation, these films may be better described as spinel-structured solid solutions. Future work may explore the broader spectrum of disorder that this implies.

Conclusion

In this work, we investigated the effect of Mg substitution on the relative stability of Ga_2O_3 polymorphs, with a particular focus on the β - and γ phases that have been experimentally observed in thin films grown on Mg-containing substrates. Our calculations indicate that Mg incorporation reduces the enthalpy differences between the different phases of Ga_2O_3 , thereby lowering the energetic barrier to forming metastable phases. For $\beta\text{-Ga}_2\text{O}_3$, Mg exhibits a strong preference for octahedral Ga sites, and this preference becomes increasingly significant at higher Mg incorporation, where octahedral substitution substantially reduces the enthalpy of formation relative to other sites. In contrast, Mg shows no clear site preference in $\gamma\text{-Ga}_2\text{O}_3$, consistent with the structural disorder of this phase. When considered alongside prior work, these results provide a mechanism for the experimentally observed stabilization of $\gamma\text{-Ga}_2\text{O}_3$ on Mg-containing substrates. More broadly, the results highlight cation substitution as a practical route to tailoring polymorph stability in Ga_2O_3 semiconductors.

Code and Data Availability Statement

Input structures, preprocessing code, and simulation input files are freely available on GitHub at https://github.com/ACME-group-CMU/Ga2O3_Mg_paper.

Acknowledgement

This research was conducted using the Tartan Research Advanced Computing Environment (TRACE). The authors would like to gratefully acknowledge the College of Engineering at Carnegie Mellon University for making this shared high-performance computing resource

available to its community. The authors acknowledge use of the Materials Characterization Facility at Carnegie Mellon University supported by Grant No. MCF-677785, and funding from the National Science Foundation (Program Manager: Yaroslav Koshka, Grant No. DMR-2324375).

Supporting Information Available

More detailed description of the process for selecting representative sets of alloy structures and associated figures.

References

- (1) Higashiwaki, M.; Sasaki, K.; Kuramata, A.; Masui, T.; Yamakoshi, S. Gallium oxide (Ga_2O_3) metal-semiconductor field-effect transistors on single-crystal β - Ga_2O_3 (010) substrates. *Applied Physics Letters* **2012**, *100*, 013504.
- (2) Green, A. J.; Chabak, K. D.; Baldini, M.; Moser, N.; Gilbert, R.; Fitch, R. C.; Wagner, G.; Galazka, Z.; Mccandless, J.; Crespo, A.; Leedy, K.; Jessen, G. H. β - Ga_2O_3 MOSFETs for Radio Frequency Operation. *IEEE Electron Device Letters* **2017**, *38*, 790–793.
- (3) Jadhav, A.; Lyle, L. A. M.; Xu, Z.; Das, K. K.; Porter, L. M.; Sarkar, B. Temperature dependence of barrier height inhomogeneity in β - Ga_2O_3 Schottky barrier diodes. *Journal of Vacuum Science & Technology B* **2021**, *39*, 040601.
- (4) Liu, A.-C.; Hsieh, C.-H.; Langpoklakpam, C.; Singh, K. J.; Lee, W.-C.; Hsiao, Y.-K.; Horng, R.-H.; Kuo, H.-C.; Tu, C.-C. State-of-the-Art β - Ga_2O_3 Field-Effect Transistors for Power Electronics. *ACS Omega* **2022**, *7*, 36070–36091, Publisher: American Chemical Society.

(5) Tang, J.; Jiang, K.; Tseng, P.-S.; Kurchin, R. C.; Porter, L. M.; Davis, R. F. Thermal stability and phase transformation of α -, κ (ε)-, and γ -Ga₂O₃ films under different ambient conditions. *Applied Physics Letters* **2024**, *125*.

(6) Yoshioka, S.; Hayashi, H.; Kuwabara, A.; Oba, F.; Matsunaga, K.; Tanaka, I. Structures and energetics of Ga₂O₃ polymorphs. *Journal of Physics: Condensed Matter* **2007**, *19*, 346211.

(7) Playford, H. Y.; Hannon, A. C.; Barney, E. R.; Walton, R. I. Structures of Uncharacterised Polymorphs of Gallium Oxide from Total Neutron Diffraction. *Chemistry – A European Journal* **2013**, *19*, 2803–2813, eprint: <https://onlinelibrary.wiley.com/doi/10.1002/chem.201203359>.

(8) Chang, C. S.; Tanen, N.; Protasenko, V.; Asel, T. J.; Mou, S.; Xing, H. G.; Jena, D.; Muller, D. A. γ -phase inclusions as common structural defects in alloyed β -(Al_xGa_{1-x})₂O₃ and doped β -Ga₂O₃ films. *APL Materials* **2021**, *9*, 051119.

(9) García-Fernández, J.; Kjeldby, S. B.; Nguyen, P. D.; Karlsen, O. B.; Vines, L.; Prytz, Ø. Formation of γ -Ga₂O₃ by ion implantation: Polymorphic phase transformation of β -Ga₂O₃. *Applied Physics Letters* **2022**, *121*, 191601.

(10) Vura, S.; Muazzam, U. U.; Kumar, V.; Vanjari, S. C.; Muralidharan, R.; Digbijoy, N.; Nukala, P.; Raghavan, S. Monolithic Epitaxial Integration of β -Ga₂O₃ with 100 Si for Deep Ultraviolet Photodetectors. *ACS Applied Electronic Materials* **2022**, *4*, 1619–1625, Publisher: American Chemical Society.

(11) Nakagomi, S.; Kokubun, Y. Crystal orientation of monoclinic β -Ga₂O₃ thin films formed on cubic MgO substrates with a γ -Ga₂O₃ interfacial layer. *Journal of Crystal Growth* **2017**, *479*, 67–74.

(12) Hou, Q.; Liu, K.; Chen, X.; Yang, J.; Ai, Q.; Cheng, Z.; Zhu, Y.; Li, B.; Liu, L.; Shen, D. Effects of Mg Component Ratio on Photode-

tection Performance of MgGa_2O_4 Solar-Blind Ultraviolet Photodetectors. *physica status solidi (RRL) – Rapid Research Letters* **2022**, *16*, 2200137, eprint: <https://onlinelibrary.wiley.com/doi/pdf/10.1002/pssr.202200137>.

(13) Hou, Q.; Liu, K.; Han, D.; Zhu, Y.; Chen, X.; Li, B.; Liu, L.; Shen, D. MOCVD growth of MgGa_2O_4 thin films for high-performance solar-blind UV photodetectors. *Applied Physics Letters* **2022**, *120*, 011101.

(14) Tang, J.; Jiang, K.; House, S. D.; Xu, C.; Xiao, K.; Porter, L. M.; Davis, R. F. Mg and Al-induced phase transformation and stabilization of Ga_2O_3 -based γ -phase spinels. *Applied Physics Letters* **2023**, *123*, 012103.

(15) Bhuiyan, A. F. M. A. U.; Feng, Z.; Johnson, J. M.; Huang, H.-L.; Sarker, J.; Zhu, M.; Karim, M. R.; Mazumder, B.; Hwang, J.; Zhao, H. Phase transformation in MOCVD growth of $(\text{Al}_x\text{Ga}_{1-x})_2\text{O}_3$ thin films. *APL Materials* **2020**, *8*, 031104.

(16) Huang, R.; Hayashi, H.; Oba, F.; Tanaka, I. Microstructure of Mn-doped $\gamma\text{-Ga}_2\text{O}_3$ epitaxial film on sapphire (0001) with room temperature ferromagnetism. *Journal of Applied Physics* **2007**, *101*, 063526.

(17) Huang, Y.; Liu, Z.; Wang, J.; Zhi, Y.; Guo, D.; Wang, X.; Wang, X.; Chen, Z.; Li, P.; Tang, W. The Effect of Mn Dopant on Structural and Optoelectronic Properties of $\gamma\text{-Ga}_2\text{O}_3$ thin Film Photodetectors. *ECS Journal of Solid State Science and Technology* **2020**, *9*, 055010, Publisher: IOP Publishing.

(18) Hayashi, H.; Huang, R.; Ikeno, H.; Oba, F.; Yoshioka, S.; Tanaka, I.; Sonoda, S. Room temperature ferromagnetism in Mn-doped $\gamma\text{-Ga}_2\text{O}_3$ with spinel structure. *Applied Physics Letters* **2006**, *89*, 181903.

(19) Huang, Y.; Gao, A.; Guo, D.; Lu, X.; Zhang, X.; Huang, Y.; Yu, J.; Li, S.; Li, P.; Tang, W. Fe doping-stabilized $\gamma\text{-Ga}_2\text{O}_3$ thin films with a high room temperature satura-

tion magnetic moment. *Journal of Materials Chemistry C* **2020**, *8*, 536–542, Publisher: The Royal Society of Chemistry.

- (20) Liu, Q.; Guo, D.; Chen, K.; Su, Y.; Wang, S.; Li, P.; Tang, W. Stabilizing the metastable γ phase in Ga_2O_3 thin films by Cu doping. *Journal of Alloys and Compounds* **2018**, *731*, 1225–1229.
- (21) Tang, J.; Jiang, K.; Xu, C.; Cabral, M. J.; Xiao, K.; Porter, L. M.; Davis, R. F. Atomic-scale investigation of $\gamma\text{-Ga}_2\text{O}_3$ deposited on MgAl_2O_4 and its relationship with $\beta\text{-Ga}_2\text{O}_3$. *APL Materials* **2024**, *12*.
- (22) Jiang, K.; Tang, J.; Xu, C.; Xiao, K.; Davis, R. F.; Porter, L. M. Evolution of $\beta\text{-Ga}_2\text{O}_3$ to $\gamma\text{-Ga}_2\text{O}_3$ solid-solution epitaxial films after high-temperature annealing. *Journal of Vacuum Science & Technology A* **2023**, *41*.
- (23) Oshima, T.; Nakazono, T.; Mukai, A.; Ohtomo, A. Epitaxial growth of $\gamma\text{-Ga}_2\text{O}_3$ films by mist chemical vapor deposition. *Journal of Crystal Growth* **2012**, *359*, 60–63.
- (24) Watanabe, T.; Miki, Y.; Masuda, T.; Deguchi, H.; Kanai, H.; Hosokawa, S.; Wada, K.; Inoue, M. Synthesis of $\gamma\text{-Ga}_2\text{O}_3\text{-Al}_2\text{O}_3$ solid solutions by spray pyrolysis method. *Ceramics International* **2011**, *37*, 3183–3192.
- (25) Peelaers, H.; Varley, J. B.; Speck, J. S.; Van de Walle, C. G. Structural and electronic properties of $\text{Ga}_2\text{O}_3\text{-Al}_2\text{O}_3$ alloys. *Applied Physics Letters* **2018**, *112*, 242101.
- (26) Seacat, S.; Lyons, J. L.; Peelaers, H. Orthorhombic alloys of Ga_2O_3 and Al_2O_3 . *Applied Physics Letters* **2020**, *116*, 232102.
- (27) Mu, S.; Van de Walle, C. G. Phase stability of $(\text{Al}_x\text{Ga}_{1-x})_2\text{O}_3$ polymorphs: A first-principles study. *Physical Review Materials* **2022**, *6*, 104601, Publisher: American Physical Society.

(28) Playford, H. Y.; Hannon, A. C.; Tucker, M. G.; Dawson, D. M.; Ashbrook, S. E.; Kastibar, R. J.; Sloan, J.; Walton, R. I. Characterization of Structural Disorder in γ -Ga₂O₃. *The Journal of Physical Chemistry C* **2014**, *118*, 16188–16198, Publisher: American Chemical Society.

(29) Gutiérrez, G.; Taga, A.; Johansson, B. Theoretical structure determination of γ -Al₂O₃. *Physical Review B* **2001**, *65*, 012101, Publisher: American Physical Society.

(30) Momma, K.; Izumi, F. VESTA 3 for three-dimensional visualization of crystal, volumetric and morphology data. *Journal of Applied Crystallography* **2011**, *44*, 1272–1276, Publisher: International Union of Crystallography.

(31) Blöchl, P. E. Projector augmented-wave method. *Physical Review B* **1994**, *50*, 17953–17979, Publisher: American Physical Society.

(32) Perdew, J. P.; Burke, K.; Ernzerhof, M. Generalized Gradient Approximation Made Simple. *Physical Review Letters* **1996**, *77*, 3865–3868, Publisher: American Physical Society.

(33) Higashiwaki, M. β -Ga₂O₃ material properties, growth technologies, and devices: a review. *AAPPS Bulletin* **2022**, *32*, 3.

(34) Marezio, M.; Remeika, J. P. Bond Lengths in the α -Ga₂O₃ Structure and the High-Pressure Phase of Ga_{2-x}Fe_xO₃. *The Journal of Chemical Physics* **1967**, *46*, 1862–1865.

(35) Cora, I.; Mezzadri, F.; Boschi, F.; Bosi, M.; Čaplovíčová, M.; Calestani, G.; Dódony, I.; Pécz, B.; Fornari, R. The real structure of ϵ -Ga₂O₃ and its relation to κ -phase. *CrysEngComm* **2017**, *19*, 1509–1516, Publisher: The Royal Society of Chemistry.

(36) Sun, W.; Ceder, G. Efficient creation and convergence of surface slabs. *Surface Science* **2013**, *617*, 53–59.

TOC Graphic

